Photocatalysis of sprayed nitrogen-containing Fe_2O_3–ZnO and WO_3–ZnO composite powders in gas-phase acetaldehyde decomposition

Di Li[*], Hajime Haneda

Electroceramics group, Advanced Materials Laboratory, National Institute for Materials Science (NIMS), 1-1 Namiki, Tsukuba 305-0044, Japan

Abstract

Two series of nano-sized N-containing MO_x–ZnO (M: Fe, W) composite powders were synthesized by spray pyrolysis. The nitrogen content was controlled from 500 to 2100 ppm by changing the powder ingredients and spray pyrolysis temperature. Ultraviolet-visible (UV-Vis) spectra indicated that the N-containing MO_x–ZnO powders absorbed not only ultraviolet light ($\lambda < 387$ nm) like pure ZnO powder, but also part of visible light ($\lambda < 650$ nm). Acetaldehyde decomposition was used as a probe reaction to evaluate the photocatalysis of these composite powders. The photocatalytic activity of the N-containing ZnO powder was pronouncedly enhanced by the WO_3 addition under both UV and visible-light irradiation. However, that of the N-containing ZnO powder was suppressed by the Fe_2O_3 addition. A model of the semiconductor energy-band structure is proposed to explain the enhancement and suppression of photocatalytic activity.
© 2003 Elsevier Science B.V. All rights reserved.

Keywords: Nitrogen-doping; Zinc oxide; Coupled semiconductors; Spray pyrolysis; Photocatalysis; Acetaldehyde

1. Introduction

The development of a photocatalyst that can work efficiently under visible-light irradiation has attracted considerable attention for hydrogen production by water splitting and the mineralization of environmental pollutants [1–4]. The approaches include the incorporation of transition metal ions (e.g. V or Cr ions) into a semiconductor powder or film by ion implantation or co-precipitation [3,5]; the introduction of oxygen vacancies by treating a photocatalyst with hydrogen plasma or X-ray irradiation [6,7]; the coupling of two semiconductors—one generally being TiO_2 or ZnO and the other semiconductor with visible-light absorption, e.g. CdS–TiO_2, WO_3–TiO_2, and SnO_2–ZnO systems—by sol–gel process; co-precipitation or simply physical mixing [8–11]; and nitrogen doping into the substitutional sites in the crystal structure of a photocatalyst, e.g. $TiO_{2-x}N_x$, TaON, $LaTaON_2$, and $LaTiO_2N$—by calcination in an ammonia atmosphere [2,4,12–14]. Obviously, the coupling of two semiconductors and nitrogen doping are likely to be the simplest methods.

In this study, we combined these two approaches by using spray pyrolysis to prepare N-containing MO_x–ZnO (M:

Fe, W) composite powders with the goal of obtaining novel ZnO-based materials with visible-light photocatalysis. We had previously used spray pyrolysis to prepare Ru/Al_2O_3 and Ru/TiO_2 thermocatalysts, and these catalysts demonstrated better performance than those prepared by conventional impregnation in the CO_2 hydrogenation [15,16]. A distinctive feature of sprayed catalysts is the homogeneous distribution of the ingredients throughout the entire particle, which occurs because all ingredients are formed from a homogeneous solution. By taking advantage of this feature, we have also synthesized deep-orange N-containing ZnO photocatalysts that can work efficiently under visible-light irradiation [17].

Photocatalytic decomposition of acetaldehyde is of great significance from the viewpoint of practical application because acetaldehyde is one of the typical bad odor-causing gases in indoor air [18,19]. Also, acetaldehyde is among the most abundant carbonyl compounds in the atmosphere [20]. Moreover, the use of ethanol-fueled vehicles popularly lead to the high levels of atmospheric acetaldehyde since the combustion of ethanol in spark-ignition engines is a primary source of acetaldehyde emission [21,22].

This paper describes two series of N-containing MO_x–ZnO composite powders (Fe_2O_3–ZnO and WO_3–ZnO) that were synthesized by spray pyrolysis. The powders were characterized by scanning electron microscopy (SEM), elemental analysis, X-ray diffraction (XRD), and ultraviolet-visible (UV-Vis) diffuse reflectance spectroscopy.

* Corresponding author. Tel.: +81-298-51-3354x727;
fax: +81-298-55-1196.
E-mail address: li.di@nims.go.jp (D. Li).

Acetaldehyde photodecomposition was used to evaluate their photocatalysis. The relationship between the characteristics of the N-containing MO_x–ZnO composite powders and their photocatalysis under both UV and visible-light irradiation is discussed.

2. Experimental

2.1. Synthesis of N-containing MO_x–ZnO powders by spray pyrolysis

High-purity ZnO (High Purity Chemicals, Japan, 99.999%) was used as the zinc source. First, the ZnO was dissolved in an ammonia aqueous solution to prepare a 0.1 M zinc–ammonia complex solution. Next, $Fe(NO_3)_3$ or $(NH_4)_{10}W_{12}O_{41}$ was added to the zinc–ammonia complex solution. A transparent solution was obtained by ultrasonic mixing for 30 min. The mixed solution was then misted by a nebulizer, and passed through a high-temperature quartz tube under the suction of an aspirator. The pyrolysis proceeded quickly (within a second) as mists passed through the high-temperature tube. The generated powder was collected with a glass filter at the end of the quartz tube.

Two series of N-containing MO_x–ZnO composite powders were prepared by changing the powder ingredients and spray pyrolysis temperatures. We call these two series as Fe-series (N-containing Fe_2O_3–ZnO composite powders) and W-series (N-containing WO_3–ZnO composite powders) and designated them as FexxNZnO-yyy and WxxNZnO-yyy, respectively. Additionally, a series of N-containing ZnO powder without MO_x, designated as NZnO-yyy, was also prepared. The "xx" indicates the amount of iron or tungsten added in weight percent, and the "yyy" represents the pyrolysis temperature in degrees Celsius.

For comparison, pure Fe_2O_3 and WO_3 powders were prepared by spray pyrolysis with a fixed pyrolysis temperature of 1027 K from $Fe(NO_3)_3$ and $(NH_4)_{10}W_{12}O_{41}$, respectively. Commercial ZnO (nanofine P-2, Sakai Chemical Industry Co., Ltd.) with a BET surface area of $50 \, m^2/g$ was used as a reference standard ZnO powder for the evaluation of the characteristics and photocatalytic performance of the sprayed N-containing ZnO and MO_x–ZnO powders. This ZnO is designated as com-ZnO.

2.2. Characterization

The particle morphology was observed with a JEOL S-5000 SEM at an acceleration voltage of 10 kV. The XRD patterns were recorded using a Philips PW1800 X-ray diffractometer with Cu Kα radiation. The UV-Vis spectra were obtained from a Jasco V-550 spectrophotometer. The BET surface area of each ZnO sample was determined by N_2 adsorption and desorption at 77 K using an automatic surface area analyzer (Model 4201, Beta Scientific Corp.). Nitrogen elemental analysis was done with a nitrogen/oxygen determinator (LECO Corporation, USA, TC-436) by heating the sample in inert gas and then using a thermal conductivity detector to analyze the obtained nitrogen.

2.3. Photocatalytic system

Photocatalytic decomposition of acetaldehyde was carried out in a closed circulation system interfaced to a gas chromatograph (Hitachi G-35A) with a TCD and a PID detector for CH_3CHO and CO_2 analysis, respectively. Prior to the catalytic experiments, the ZnO samples (0.0500 g) were outgassed under vacuum of 10^{-5} Pa at 398 K for 2.0 h. A gas mixture of 88.0 kPa CH_3CHO–He (790 ppm) and 13.3 kPa O_2 was then introduced. The samples were irradiated from outside of the reactor. A 200 W Hg–Xe lamp (LA-300UV, $\lambda_{max} = 365$ nm) and a 150 W Xe lamp (LA-254Xe, $\lambda_{max} = 470$ nm, Hayashi Watch-Works. Co., LTD, Japan) were used as the UV and visible light sources, respectively. The wavelength of the visible light was controlled through a 390 and 420 nm cut filter (L39, L42, Kenko, Japan). The incident intensity to the sample surface for both light sources was set up to be 20 mW cm^{-2}.

3. Results and discussion

3.1. Characterization of N-containing MO_x–ZnO powders

3.1.1. Morphology
The SEM images of some typical samples are shown in Fig. 1. A similar morphology was observed irrespective of the addition of MO_x. These were hollow spherical particles with open, microscopic surface porosity, and the shells of the hollow particles consisted of nano-sized crystallites (primary particles). However, for the Fe0.7NZnO-800 and W5.8NZnO-800 samples, the particles had a more regularly spherical shape and the size of the primary particles was much smaller than for the NZnO-800 (with no MO_x added). Obviously, the MO_x inhibited the primary particle growth of ZnO. The sizes of the primary particles were about 31 nm for Fe0.7NZnO-800, 15 nm for W5.8NZnO-800, and 45 nm for NZnO-800.

3.1.2. Nitrogen content and BET surface area
The chemical composition of the synthesized powders was determined by elemental analysis. Prior to the elemental analysis, all as-sprayed samples were calcined at 873 K for 2 h to ensure that any possible residual precursors would decompose completely. The nitrogen atoms in the calcined samples were considered as site-nitrogen; i.e. nitrogen atoms that were doped into the oxygen sites of the ZnO crystal lattice [17].

The results of the elemental analysis and the BET surface area of some samples are listed in Table 1. Firstly, the
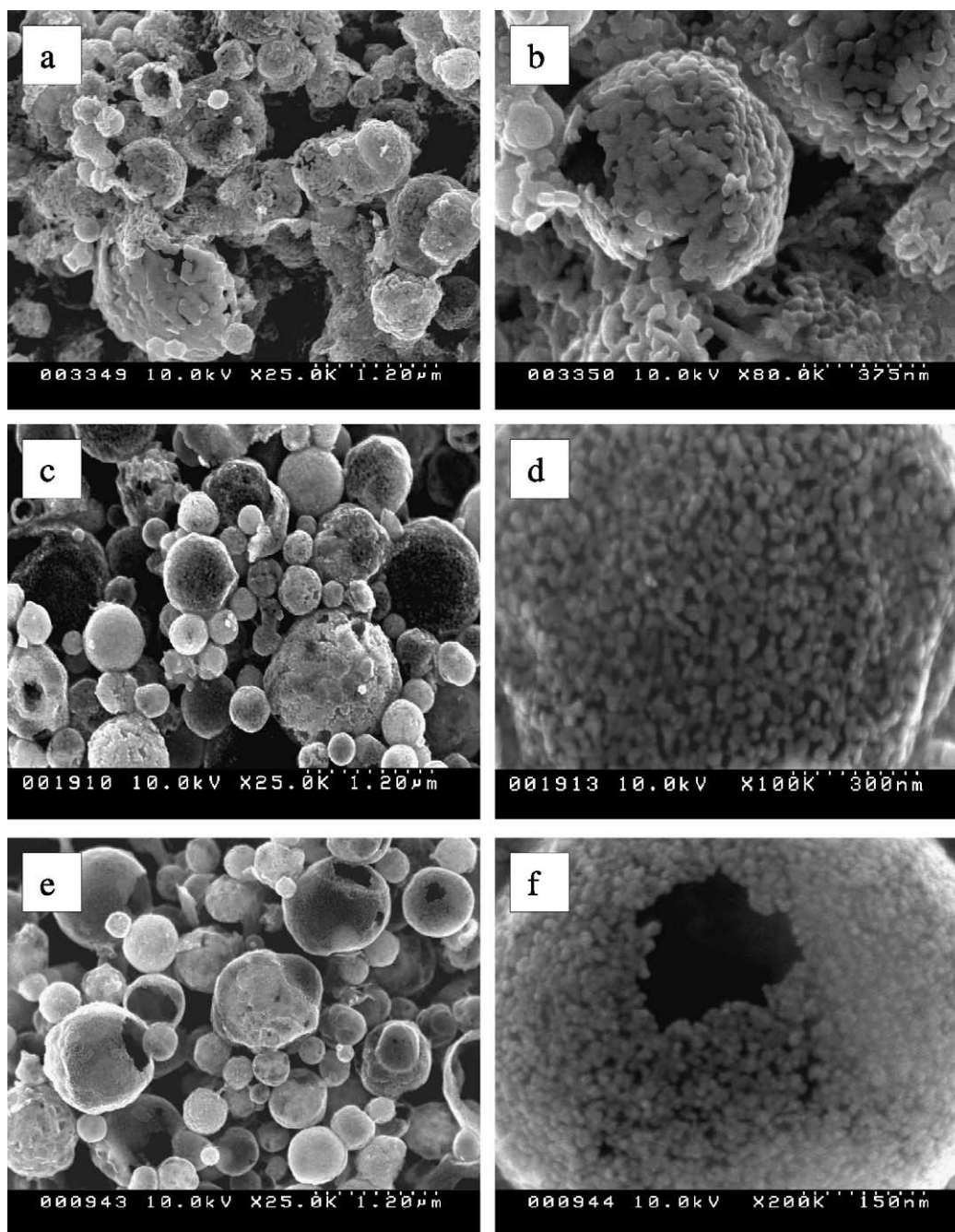
Fig. 1. SEM images of NZnO-800 (a, b), Fe0.7NZnO-800 (c, d), and W5.8NZnO-800 (e, f) powders.

pyrolysis temperature had a great effect on the nitrogen content irrespective of the MO_x addition. Secondly, by comparing the nitrogen contents of NZnO and W-series samples prepared at the same pyrolysis temperature, e.g. NZnO-800 and W5.8NZnO-800, we can conclude that the nitrogen content was greatly increased by WO_3 addition. The nitrogen content also increased monotonically with increasing tungsten additive amounts, but the extent of the increase was significantly smaller than the increase in the WO_3 additive amount, e.g. it increased only by 11% (from 1900 to 2100 ppm) when the tungsten additive amount increased by

81% (from 5.8 to 10.5%). This indicates that the increased nitrogen content caused by the WO_3 introduction did not originate from the formation of tungsten nitride or oxynitride. On the contrary, the nitrogen content almost did not change at all when Fe_2O_3 was added, even when the iron was increased to 1.7%. Accordingly, the nitrogen contents ranged from 1200 to 2100 ppm for W-series powders and from 500 to 1000 ppm for Fe-series powders.

The WO_3 or Fe_2O_3 addition to ZnO induced an appreciable change in the surface area, and the BET surface area increased with increasing additive amount. Kwon et al.

Table 1
Summary of elemental analysis (wt.%), BET surface area, and water content of N-containing MO_x–ZnO composite powders

Sample	N (ppm)	Fe or W (wt.%)	O (wt.%)	Zn (wt.%)	H_2O (wt.%)	BET (wt.%)
Fe0.7NZnO-600	1000	0.72	21.5	77.6	2.3	55
Fe0.7NZnO-800	700	0.69	21.0	78.2	1.6	45
Fe0.7NZnO-1000	500	0.70	20.7	78.6	1.1	37
Fe0.4NZnO-800	700	0.35	20.6	78.9	1.2	51
Fe1.7NZnO-800	600	1.7	21.5	76.9	1.8	30
W5.8NZnO-600	1500	5.9	21.2	72.5	1.2	58
W5.8NZnO-800	1900	5.8	20.4	73.5	1.0	49
W5.8NZnO-1000	1200	5.7	20.2	73.9	0.7	39
W3.2NZnO-800	1600	3.2	20.2	76.3	0.8	42
W10.5NZnO-800	2100	10.5	20.7	68.5	1.3	53
NZnO-600	1100		21.0	78.3	1.8	50
NZnO-800	600		20.5	79.4	0.7	39
NZnO-1000	400		20.3	79.7	0.7	33

observed a similar tendency in the WO_3–TiO_2 system [23]. Note that the BET surface area of some of our sprayed samples exceeded that of com-ZnO ($50 \, m^2 \, g^{-1}$), which is generally regarded as the commercial ZnO powder with the highest BET surface area. This indicates that spray pyrolysis should be a feasible method for preparing N-containing powders with high surface areas.

3.1.3. Structure

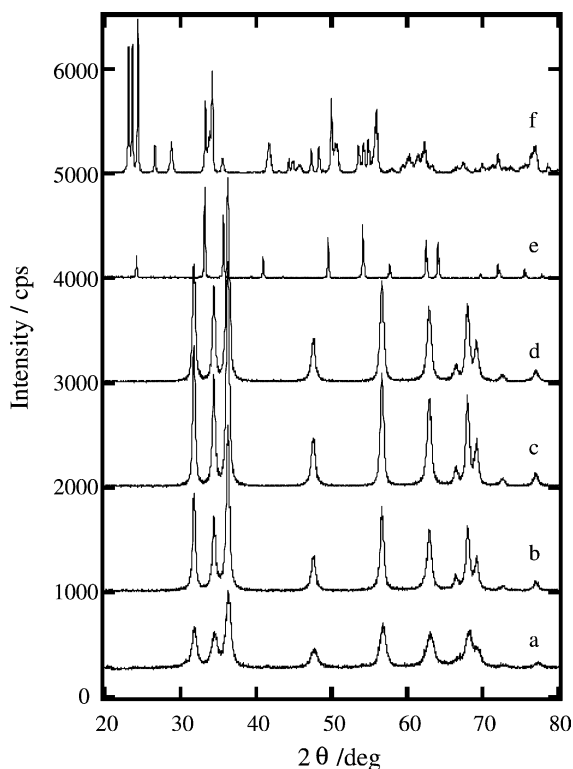XRD patterns of some selected samples are shown in Fig. 2. All diffraction peaks in Fig. 2a–d could be identified

Fig. 2. XRD patterns of some typical samples and references. (a) W5.8NZnO-800; (b) Fe0.7NZnO-800; (c) NZnO-800; (d) com-ZnO; (e) Fe_2O_3; and (f) WO_3.

as a ZnO phase with a hexagonal wurtzite crystal structure. Peaks related to iron or tungsten oxides were not observed in MO_x-added samples (Fig. 2a and b), suggesting that the MO_x was well dispersed in the ZnO particles. As mentioned above, this is a distinctive feature of the sprayed powders. Additionally, no nitrogen-related compounds (e.g. Zn_3N_2) were found; their content was too low to allow detection of their reflection peaks. Moreover, the formation of α-Fe_2O_3 (Fig. 2e) and WO_3 (Fig. 2f) phases was confirmed from their corresponding precursor $Fe(NO_3)_3$ and $(NH_4)_{10}W_{12}O_{41}$ by spray pyrolysis. This would indicate that the added iron existed in the form of α-Fe_2O_3 and the tungsten was in the form of WO_3. The $ZnFe_2O_4$ or $ZnWO_4$ new phase did not appear until the spray pyrolysis temperature was up to 1473 K (we did not show their XRD results for the sake of brevity).

The crystallite sizes obtained from the 102 peak of the XRD pattern were about 29.8 nm for Fe0.7NZnO-800, 13.5 nm for W5.8NZnO-800, and 41.2 nm for NZnO-800. These values are almost identical to those of the observed primary particles (Fig. 1).

3.1.4. Optical property

The UV-Vis spectra of the sprayed N-containing MO_x–ZnO composite powders, and, for comparison, those of the NZnO, com-ZnO, WO_3, and Fe_2O_3, were recorded by the diffuse reflectance technique. $BaSO_4$ was used as a reference to measure all the samples.

Figs. 3 and 4 show the dependence of the absorption spectra of the N-containing MO_x–ZnO powders on pyrolysis temperature and MO_x additive amount, respectively. Two absorption edges were observed for all N-containing samples. The UV absorption edge at about 385 was ascribed to the fundamental absorption of ZnO. Obviously, nitrogen introduction and MO_x addition did not remarkably affect the UV absorption of ZnO. The other absorption edge was in the visible range at about 500 nm and changed very little with the pyrolysis temperature. We attribute this absorption edge to nitrogen introduction rather than MO_x addition, although the coupling of MO_x–ZnO can also extend the spectral response of ZnO into the visible region. This conclusion was
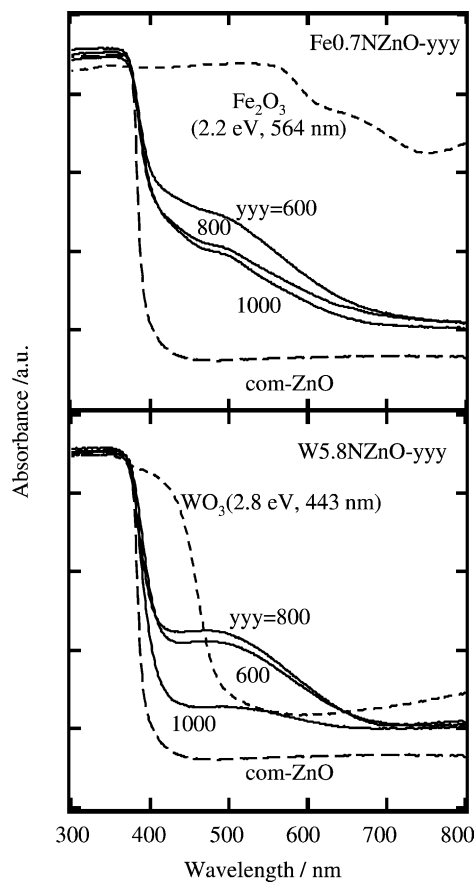
Fig. 3. UV-Vis adsorption spectra of Fe0.7NZnO and W5.8NZnO powders prepared at different pyrolysis temperature.

Fig. 4. UV-Vis adsorption spectra of FexxNZnO-800 and WxxNZnO-800 powders with different additive amounts of iron or tungsten.

made based on the following experimental results: this absorption edge does not agree with that of the sprayed Fe_2O_3 or WO_3 powders (Fig. 3); the band-gap was 2.2 V for the Fe_2O_3 and 2.8 eV for the WO_3, and these values are consistent with those reported in the literature [24,25]. This absorption edge corresponds to a band-gap of about 2.5 eV, which falls within the range of that observed for a zinc oxynitride ($Zn_xO_yN_z$) thin film, where the optical band-gap decreases from 3.26 to 2.30 eV when the nitrogen concentration in the films is increased from 0 to 10 at.% [26]. For our synthesized N-containing MO_x–ZnO composite powders, the nitrogen atoms are considered to be doped into the part of ZnO lattice sites instead of oxygen atoms since these samples are deep-orange, and the color is slightly changed even after the samples were calcined at 873 K for 2 h.

It also can be concluded from Fig. 3 that the optimal pyrolysis temperatures for obtaining the maximum visible-light absorption were 873 K for Fe-series powders and 1073 K for W-series powders. The highest nitrogen content was also achieved at this temperature (Table 1), indicating that visible-light absorption is closely related to nitrogen content. Moreover, the results in Fig. 4 indicate that the iron or tungsten additive amount had a pronounced effect on the visible-light absorption, except in the sample with higher tungsten content.
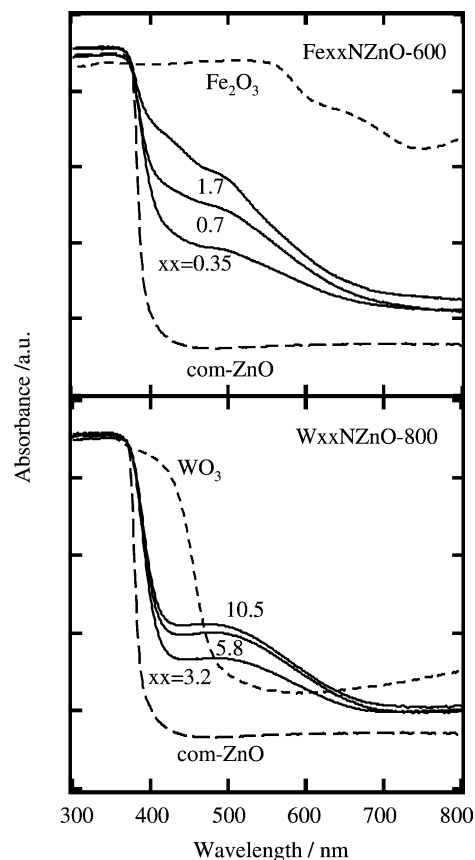
The absorption spectra of Fe0.7NZnO-600, NZnO-600, W5.8NZnO-800, NZnO-800, and com-ZnO are summarized in Fig. 5 for comparison. Our results indicate that MO_x addition significantly improves the visible-light absorption of NZnO powder. Here, it is worth noting that this improvement originated from the increase of the nitrogen content
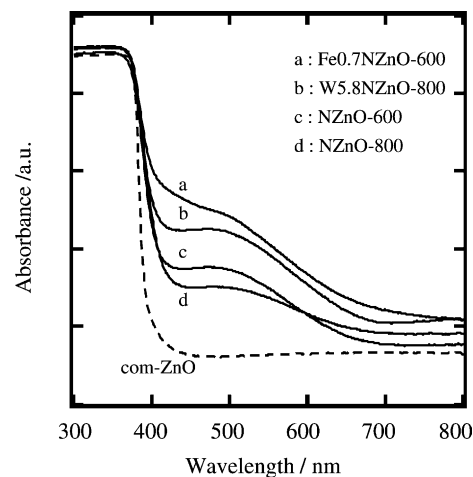

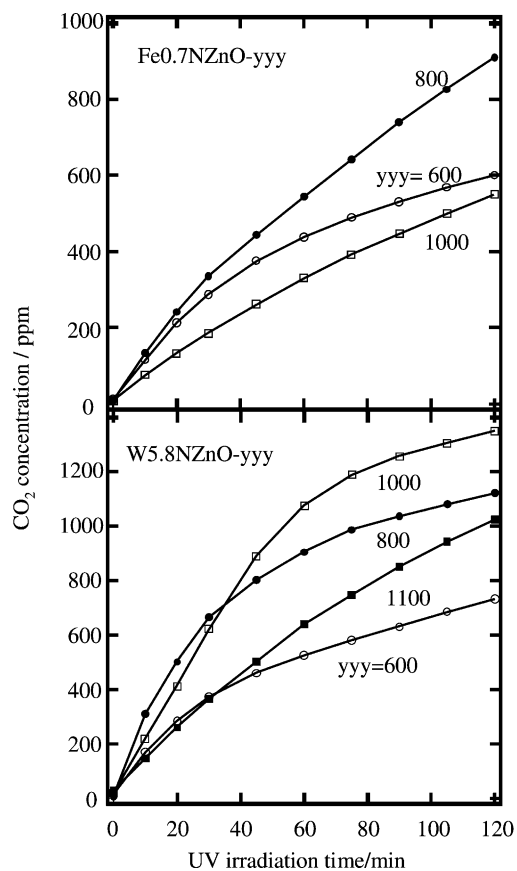Fig. 5. UV-Vis adsorption spectra of some selected samples and references.

Fig. 6. CO_2 evolution from the UV photocatalytic decomposition of acetaldehyde on Fe0.7NZnO and W5.8NZnO powders prepared at different pyrolysis temperatures.

Fig. 7. CO_2 evolution from the UV photocatalytic decomposition of acetaldehyde on FexxNZnO-800 and WxxNZnO-800 powders.

caused by WO_3 introduction and the added WO_3 itself for the W-series powders and only from the added Fe_2O_3 for the Fe-series powders, since the nitrogen content kept unchangeable after the Fe_2O_3 addition.

3.2. Photocatalysis of N-containing MO_x–ZnO composite powders

3.2.1. Photocatalytic activity under UV irradiation

The dependence of the UV photocatalysis of sprayed N-containing MO_x–ZnO powders on the pyrolysis temperature and the iron or tungsten additive amount were investigated in order to determine the optimal conditions for sample preparation. The observed results are shown in Figs. 6 and 7. We concluded that both the pyrolysis temperature and the iron or tungsten additive amount significantly affect the photocatalytic activity of N-containing MO_x–ZnO photocatalysts, and that, if the CO_2 concentration 2 h after the reaction began is representative of the photocatalytic activity, the highest photocatalytic activity can be obtained on Fe0.7NZnO-800 for the Fe-series powders and W5.8NZnO-1000 for the W-series powders, i.e. the optimal pyrolysis temperature and additive amount were 1073 K and 0.7% for the Fe-series photocatalysts, and 1273 K and
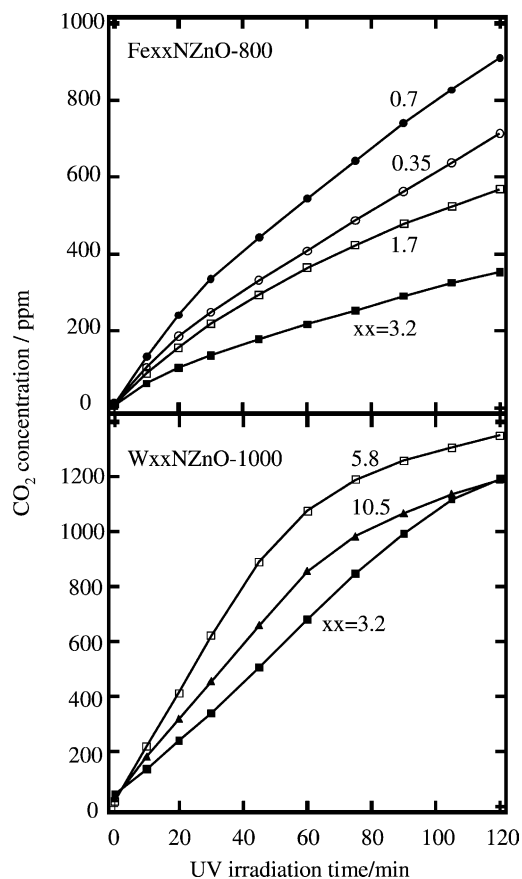
5.8% for the W-series photocatalysts. These optimal conditions did not agree with the ones at which the maximum nitrogen contents were obtained for both series of powders, indicating that the nitrogen content perhaps has no direct relationship with the UV photocatalysis of ZnO powders.

In general, the catalytic activity of a photocatalyst should be closely related to its crystal structure, crystallinity, BET surface area, surface hydroxyl group density, oxygen vacancies, and so on [27–29]. The dependence of the photocatalytic activity of N-containing MO_x–ZnO powders on pyrolysis temperature seems to be a synthetic result that reflects these factors. On one hand, the improvement in crystallinity with increasing pyrolysis temperature should enhance the photocatalytic activity since the concentration of crystal defects, which may act as centers of charge carrier recombination, falls as the level of crystallinity rises [30,31]. On the other hand, at higher pyrolysis temperatures, the morphology and surface properties of the particles might change due to sintering, and this would result in the decrease not only in the BET surface area (Table 1) but also in the surface hydroxyl group density [32]. The decrease in the BET surface area might reduce the reactant adsorption, while that of the surface hydroxyl group would seriously affect the formation of hydroxyl radicals ($^\bullet$OH) since this active species is generated via hole capture by the surface
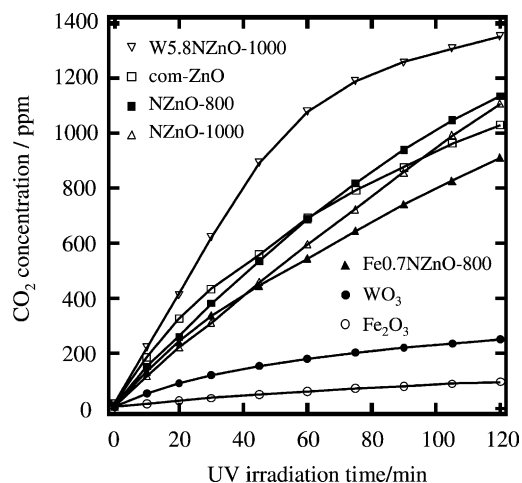
Fig. 8. UV photocatalytic activities over some selected photocatalysts and references.

Fig. 9. CO_2 evolution during the visible-light ($\lambda > 390$ nm) photocatalytic decomposition of acetaldehyde on some selected samples and references.

hydroxyl [33,34]. The suppression of photocatalytic activity for the samples prepared at higher pyrolysis temperatures should be associated with decreases of both the BET surface area and the surface hydroxyl. As for the optimal Fe_2O_3 and WO_3 additive amounts, other researchers also observed a similar result [9,35]. An optimal charge carrier separation distance was proposed to explain it by Sadeghi et al. [36].

Additionally, the shapes of the CO_2 time-course curves in Fig. 6 obviously differ. For some samples prepared at a lower pyrolysis temperature (e.g. at 873 K), the CO_2 concentration increased exponentially with irradiation time, especially within 1.0 h after the reaction started. However, for some samples prepared at a higher pyrolysis temperature (e.g. at 1273 K), the CO_2 concentration increased linearly. This distinctive difference in the shape of the CO_2 time-course curves probably means that the acetaldehyde decomposition occurred through different reaction mechanisms [33,37].

The photocatalytic activities of the optimal N-containing MO_x–ZnO composite powders and those of some reference samples are summarized in Fig. 8. These results indicate that WO_3 addition significantly enhanced the photocatalytic activity of N-containing ZnO powders (comparing W5.8NZnO-1000 with NZnO-1000). On the contrary, Fe_2O_3 addition suppressed the photocatalytic activity (comparing Fe0.7NZnO-800 with NZnO-800). We will later propose a model of the semiconductor energy-band structure to explain this. In addition, an obvious change in photocatalytic activity was not observed between NZnO-800 or NZnO-1000 and com-ZnO, indicating that nitrogen introduction has a mi-
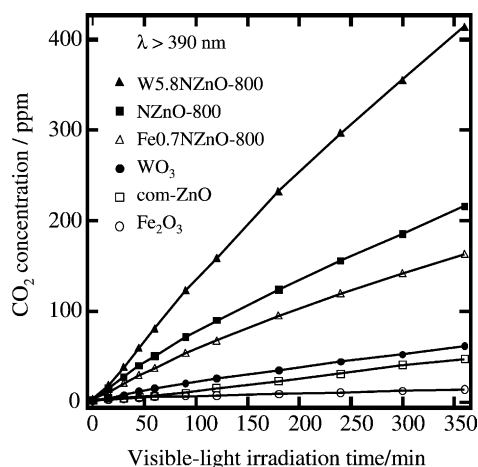
nor effect on the UV photocatalysis of ZnO. Moreover, the Fe_2O_3 or WO_3 powder had a lower photocatalytic activity for acetaldehyde decomposition, suggesting that the oxidative ability of the MO_x–ZnO composite powders seems to be governed by ZnO, and the MO_x serves as an associated photocatalyst.

With regard to the UV photocatalytic activity of some samples, we also calculated the initial rates of CO_2 formation, CO_2 yields, and quantum yields 1 h after the reaction began through the time-course curve of CO_2 evolution. These are summarized in Table 2.

3.2.2. Photocatalytic activity under visible-light irradiation

Fig. 9 shows the CO_2 evolutions over some samples with the visible-light irradiation longer than 390 nm. These samples were prepared at a fixed pyrolysis temperature of 1073 K for comparison. The photocatalytic activity of NZnO-800 was much higher than that of com-ZnO, indicating that visible-light photocatalysis of ZnO was greatly improved by the nitrogen introduction. This differs from the UV case. Nevertheless, such improvement was further enhanced by the WO_3 addition, confirming that the coupling of ZnO with WO_3 is an effective way to prepare ZnO-based materials with visible-light photocatalysis. However, a contrary result was observed for the Fe_2O_3 addition.

The photocatalytic activities of some samples under visible-light irradiation longer than 420 nm were also examined and showed in Fig. 10, but the results were similar to those for the 390 nm case.

Table 2
UV photocatalytic activities of some selected samples

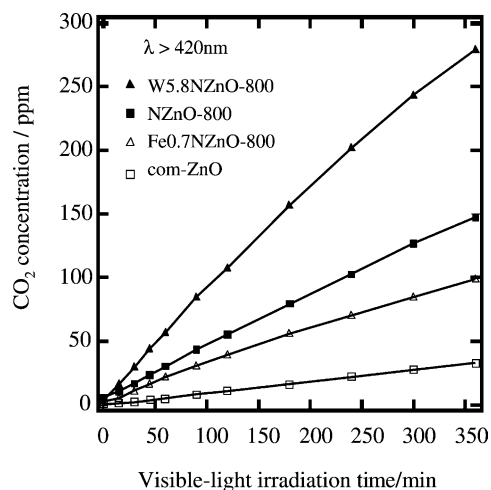| Photocatalytic activity	Fe0.7NZnO-800	W5.8NZnO-1000	NZnO-800	NZnO-1000	com-ZnO	WO$_3$	Fe$_2$O$_3$
R_0 (10^{-7} mol min^{-1})	1.1	3.9	1.6	1.4	1.8	0.59	0.11
CO_2 yield (%)	39.7	78.4	50.1	43.3	51.0	13.1	4.5
Quantum yield (%)	2.0	3.9	2.4	2.1	2.5	0.65	0.22

Fig. 10. CO_2 evolution during the visible-light ($\lambda > 420$ nm) photocatalytic decomposition of acetaldehyde on some selected samples and references.

The quantum yields for CO_2 formation 6 h after the visible-light irradiation longer than 390 nm were calculated for the NZnO-, Fe0.7NZnO-, and W5.8NZnO-series photocatalysts prepared at different pyrolysis temperature in order to fully investigate the effect of pyrolysis temperature on the visible-light photocatalytic activity. The results are summarized in Fig. 11. The photocatalytic activity of NZnO powders was enhanced through the WO_3 addition and suppressed through the Fe_2O_3 addition no matter what pyrolysis temperature was used. The optimal quantum yield was obtained on Fe0.7NZnO-600 for Fe-series photocatalysts, and on W5.8NznO-800 for W-series photocatalysts. These results are quite consistent with the corresponding nitrogen contents, suggesting that the visible-light photocatalysis of these powders is closely related to nitrogen doping. We ascribe this enhancement of visible-light photo-
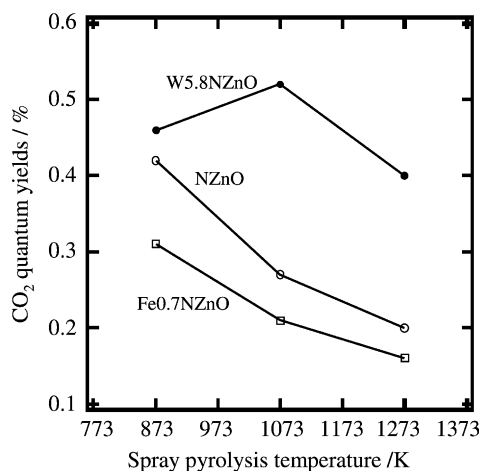

Fig. 11. Dependence of the CO_2 quantum yields on pyrolysis temperatures over Fe0.7NZnO-yyy (a), W5.8NZnO-yyy (b), NZnO-yyy (c) powders under visible-light ($\lambda > 390$ nm) irradiation.

catalytic activity of NZnO powder through WO_3 addition to two factors. One is that WO_3 addition increases the nitrogen content in the samples and further improves the absorption of visible light. This is a prerequisite for a photocatalyst to be able to catalyze a reaction under visible-light irradiation. However, it should be noted that even though a photocatalyst can absorb a greater quantity of visible light, it does not mean it will have good visible-light photocatalytic performance; the suppression of photocatalytic activity of NZnO powders by Fe_2O_3 addition supports this conclusion. The second is that the WO_3 addition facilitates effective separation of photo-generated electrons and holes as we will discuss below.

3.2.3. Photocatalytic mechanisms of N-containing ZnO powders by MO_x addition

The coupling of two semiconductors possessing different redox energy levels for their corresponding conduction bands (CB) and valence bands (VB) is an attractive approach to achieve more efficient charge separation, increase the lifetime of charge carriers, and enhance the efficiency of the interfacial charge transfer to adsorbed reactants. However, the relative positions of the CBs and VBs of the two selected semiconductors are vitally important for obtaining the expected results.

The principle of charge separation is illustrated in Fig. 12 by our proposed energy-band structure models for the N-containing MO_x–ZnO composite photocatalysts. The relative positions of the CBs and VBs of ZnO, WO_3 and Fe_2O_3 were determined from the following values versus NHE at pH 7: CB of $+0.2$ V and VB of $+2.4$ V in Fe_2O_3 ($E_g = 2.2$ eV) [38], CB of $+0.4$ V and VB of $+3.2$ V in WO_3 ($E_g = 2.8$ eV) [39], and CB of -0.5 V and VB of $+2.7$ V in ZnO ($E_g = 3.2$ eV) [40]. Fujii et al. [24] and Serpone et al. [25] also summarized these values in their publications.

For the UV irradiation, we only considered the coupling effect of MO_x–ZnO since nitrogen introduction has a minor influence on the UV photocatalytic activity (Fig. 12a). The electrons in the VB of ZnO can first be excited to the CB of ZnO by UV irradiation, and then the excited electrons will transfer to the CB of WO_3 since the CB of WO_3 is lower than that of ZnO. On the other hand, the holes in the VB of excited WO_3 can transfer to the VB of ZnO since the VB of ZnO is higher than that of WO_3. This means that the WO_3 acts as a sink for the photogenerated electrons. Tennakone et al. reported that the W(VI) in WO_3 can be easily reduced to W(V) [41]. Therefore, the electrons transferred from the CB of ZnO to the CB of WO_3 will prefer to reduce W(VI) to W(V). Furthermore, the W(V) is oxidized to the original W(VI) by the adsorbed oxygen on the surface of WO_3. Through these redox reactions, the electrons that originated from the VB of ZnO are indirectly transported to the adsorbed oxygen on the surface of WO_3, and therefore the recombination of photogenerated electrons and holes is avoided. On the contrary, the Fe_2O_3–ZnO system
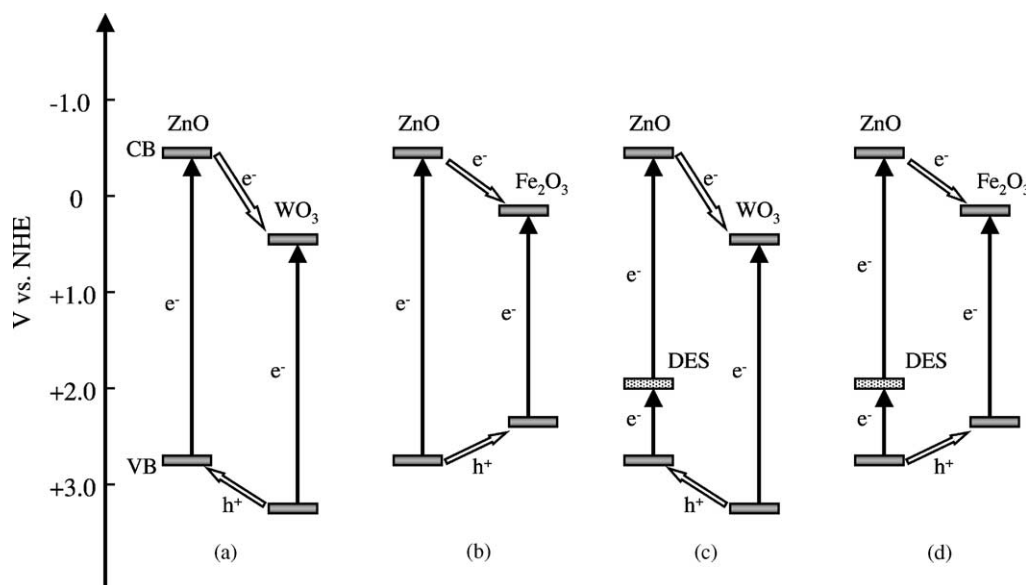
Fig. 12. Proposed principles of the charge separation for the coupled WO_3–ZnO (a, c) and Fe_2O_3–ZnO (b, d) systems under both UV (a, b) and visible-light (c, d) irradiation.

(Fig. 12b) is rather unique in that both CB and VB of Fe_2O_3 are sandwiched between the corresponding bands of ZnO. Thus, simultaneous excitation of both components can lead to a one-way transfer of both electrons and holes from ZnO semiconductor to Fe_2O_3; the latter is a less efficient photocatalyst than its counterpart under identical conditions. Accordingly, the Fe_2O_3 acts as a sink for both photogenerated electrons and holes, and cannot improve the separation of charge carrier originated from ZnO excitation.

For the visible-light case, we considered not only the coupling effect of MO_x–ZnO but also the N-doping effect. Firstly, the doped nitrogen content is too low to change the band-gap of ZnO; instead a new absorption band appears in the visible-light range (Figs. 3–5). Hence, we believe that a defect energy state (DES) is newly formed by N-doping between the VB and CB in the ZnO band structure, and the DES should be close to the VB of ZnO since the energy levels of the nitrogen 2p orbitals is higher than that of oxygen (Fig. 12c) [42]. The electrons generated in the VB of ZnO by visible-light irradiation ($h\nu > 0.7$ eV) could have been first excited to the DES, and then further transferred to the CB of ZnO by absorbing more energy ($h\nu > 2.5$ eV) than that of the first step transition. This means that, since a DES is formed, the electron transition from VB to CB in a ZnO semiconductor, generally produced by UV irradiation ($h\nu > 3.2$ eV), can be achieved through two-step transitions even with the lower energy of visible-light irradiation. The DES acts like an "energy supply station" for the excited electrons. Secondly, the excited electrons in the CB of ZnO would have been transferred to the CB of WO_3, and the WO_3 would still act as a sink for the photogenerated electrons. For the Fe_2O_3–ZnO system (Fig. 12d), the Fe_2O_3 works as in its UV case.

In our proposed medal, we mainly considered the transitions of the excited electrons and holes located in the VB of the ZnO semiconductor since they governed the oxidative ability of the composite photocatalysts. Additionally, the electrons in the DES could be excited to the CB of ZnO by absorbing visible light ($h\nu > 2.5$ eV), then transferred to the CB of WO_3 or Fe_2O_3, however, a high oxidative ability was not expected for these excited electrons since the DES level is higher than the VB of ZnO with 0.7 eV.

4. Conclusions

The feasibility of spray pyrolysis for preparing nano-sized N-containing MO_x–ZnO powders with large surface area has been demonstrated. These sprayed powders comprised hollow spherical particles with open, microscopic surface porosity, and the shells of the sprayed particles consisted of nano-scale crystallites. The concentration of nitrogen significantly depended on the pyrolysis temperature and ranged from 500 to 2100 ppm. The N-containing MO_x–ZnO composite powders absorbed not only ultraviolet light like pure ZnO powder but also part of visible light. The photocatalytic activity of the N-containing ZnO powder was greatly enhanced by the WO_3 addition under both UV and visible-light irradiation. This enhancement was ascribed to the WO_3 acting as a sink for photogenerated electrons in the UV case, and to a synergistic effect of N-doping and WO_3–ZnO coupling in visible-light case. On the contrary, the photocatalytic activity of the N-containing ZnO powder was suppressed by the Fe_2O_3 addition since Fe_2O_3 acts as a center of photogenerated electron and hole recombination.

Consequently, N-containing WO$_3$–ZnO composite photocatalysts were developed that are capable of working efficiently under visible-light irradiation. The practical application of these novel materials, such as in photocatalytic deodorization systems and antibacterial agents, is of further interest.

Acknowledgements

References

[1] G. Hitoki, T. Takada, J.N. Kondo, M. Hara, H. Kobayashi, K. Domen, Chem. Comm. (2002) 1698.

[2] T. Ohno, F. Tanigawa, K. Fujishima, S. Izumi, M. Matsumura, J. Photochem. Photobio. A. Chem. 118 (1998) 41.

[3] M. Anpo, Pure Appl. Chem. 72 (2000) 1787.

[4] R. Asahi, T. Morikawa, T. Ohwaki, K. Aoki, Y. Taga, Science 392 (2001) 269.

[5] D. Dvoranová, V. Brezová, M. Mazúr, M.A. Malati, Appl. Catal. B: Environ. 37 (2002) 91.

[6] I. Nakamura, N. Negishi, S. Kutsuna, T. Ihara, S. Sugihara, K. Takeuchi, J. Mol. Catal. A: Chem. 161 (2000) 205.

[7] S. Iimura, H. Teduka, A. Nakagawa, S. Yoshihara, T. Shirakashi, Electrochem. 69 (5) (2001) 324.

[8] K.R. Gopidas, M. Bohorquez, P.V. Kamat, J. Phys. Chem. 94 (1990) 6435.

[9] X. Li, F. Li, C. Yang, W. Ge, J. Photochem. Photobiol. A: Chem. 141 (2001) 209.

[10] A. Fuerte, M.D. Hernándze-Alonso, A.J. Maira, A. Martínez-Arias, M. Fernándze-García, J.C. Conesa, J. Soria, G. Munuera, J. Catal. 212 (2002) 1.

[11] C. Wang, J. Zhao, X. Wang, B. Bai, G. Sheng, P. Peng, J. Fu, Appl. Catal. B: Environ. 39 (2002) 269.

[12] S. Sato, Chem. Phys. Lett. 123 (1986) 126.

[13] M. Jansen, H.P. Letschert, Nature 404 (2000) 980.

[14] A. Kasahara, K. Nukumizu, G. Hitoki, T. Takada, J.N. Kondo, M. Hara, H. Kobayashi, K. Domen, J. Phys. Chem. A. 106 (2002) 6750.

[15] D. Li, N. Ichikuni, S. Shimazu, T. Uematsu, Appl. Catal. A: Gen. 172 (1998) 351.

[16] D. Li, N. Ichikuni, S. Shimazu, T. Uematsu, Appl. Catal. A: Gen. 180 (1999) 227.

[17] D. Li, H. Haneda, J. Photochem. Photobiol. A: Chem. 155 (2003) 171.

[18] G. Leonardos, D. Kendall, N. Barnard, J. Air Pollut. Control Assoc. 19 (1969) 91.

[19] H. Wakeham, in: I. Schmeltz (Ed.), The Chemistry of Tabacoo Smoke, Plenum Press, New York, 1972, p. 1.

[20] L.G. Anderson, J.A. Lanning, R. Barrell, J. Miyagishima, R.H. Jone, P. Wolfe, Atmos. Environ. 30 (1996) 2113.

[21] D. Grosjean, A.H. Miguel, T. Tavares, Atmos. Environ. 24B (1990) 101.

[22] J.S. Gaffney, N.A. Marley, R.S. Martin, R.W. Dixon, L.G. Reyes, C.J. Popp, Environ. Sci. Technol. 31 (1997) 3053.

[23] Y.T. Kwon, K. Song, W. Lee, G. Choi, Y. Do, J. Catal. 191 (2000) 192.

[24] M. Fujii, T. Kawai, S. Kawai, Chem. Phys. Lett. 106 (6) (1984) 517.

[25] N. Serpone, P. Maruthamuthu, P. Pichat, E. Pelizzetti, H. Hidaka, J. Photochem. Photobio. A: Chem. 85 (1995) 347.

[26] M. Futsuhara, K. Yoshioka, O. Takai, Thin Solid Films 317 (1998) 322.

[27] D. Li, H. Haneda, Chemosphere 51 (2003) 129.

[28] M.A. Fox, M.T. Dulay, Chem. Rev. 93 (1997) 341.

[29] B. Ohtani, Y. Ogawa, S. Nishimoto, J. Phys. Chem. B 101 (1997) 3746.

[30] G.R. Bamwenda, H. Arakawa, Appl. Catal. A: Gen. 210 (2001) 181.

[31] T. Hirakawa, H. Kominami, B. Ohtani, Y. Nosaka, J. Phys. Chem. B 105 (2001) 6993.

[32] L. Jing, Z. Xu, X. Sun, J. Shang, W. Cai, Appl. Surf. Sci. 180 (2001) 308.

[33] Y. Ohko, D.A. Tryk, K. Hashimoto, A. Fujishima, J. Phys. Chem. B 102 (1998) 2699.

[34] M.I. Litter, Appl. Catal. B: Environ. 23 (1999) 89.

[35] S. Sakthivel, S.-U. Geissen, D.W. Bahnemann, V. Murugesan, A. Vogelpohl, J. Photochem. Photobiol. A: Chem. 148 (2002) 283.

[36] M. Sadeghi, W. Liu, T.-G. Zhang, P. Stavropoulos, B. Levy, J. Phys. Chem. B 100 (1996) 19466.

[37] I. Sopyan, M. Watanabe, S. Murasawa, K. Hashimoto, A. Fujishima, J. Photochem. Photobiol. A: Chem. 98 (1996) 79.

[38] A.J. Nozik, Ann. Rev. Phys. Chem. 29 (1978) 189.

[39] D.E. Scaife, Solar Energy 25 (1980) 41.

[40] G. Redmond, A. Okeeffe, C. Burgess, C. MacHale, D. Fitzmaurice, J. Phys. Chem. 97 (1993) 11081.

[41] K. Tenakone, O.A. Heperuma, J.M.S. Bandara, W.C.B. Kiridena, Semicon. Sci. Technol. 7 (1992) 423.

[42] R. Marchand, F. Tessier, A. Le Sauze, N. Diot, Inter. J. Inorg. Mater. 3 (2001) 1143.